







Experimental evaluation of the efficiency of a pneumatic strain energy accumulator

Joshua J. Cummins^a, Seth Thomas^b , Christopher J. Nash^a , Sankaran Mahadevan^c , Douglas E. Adams^c and Eric J. Barth^{a,d} 

^aMechanical Engineering, Vanderbilt University, Nashville, TN, USA; ^bApplied Physics, University of Central Arkansas, Conway, AR, USA; ^cCivil and Environmental Engineering, Vanderbilt University, Nashville, TN, USA; ^dLaboratory for the Design and Control of Energetic Systems (DCES), Vanderbilt University, Nashville, TN, USA

ABSTRACT

There is heightened interest in research to develop materials and devices that achieve greater energy storage capacity, power density and increased energy efficiency. This work analyses the performance of a novel energy storage device, the pneumatic strain energy accumulator (pSEA), which is designed to exploit the advantageous aspects of the non-linear behaviour of elastomeric materials. An analytical method for simultaneously characterising the pneumatic energy and strain energy stored in a strain energy accumulator (SEA), and more generally for pneumatic and strain energy systems, has been employed. Component efficiency along with the expansion and contraction pressures of the pSEA are determined experimentally so that a system level efficiency calculation can be performed. Incorporating uncertainty analysis, the efficiencies of the SEA are measured to be consistently over 93% in over 800 cycles of testing. The steady-state expansion and contraction pressures of the accumulator have steady-state values with errors of less than 3 hundredths of a kilopascal from their means.

ARTICLE HISTORY

Received 26 February 2016
Accepted 20 May 2017

KEYWORDS

Strain energy accumulator; efficiency; uncertainty analysis; pneumatic; energy saving

1. Introduction

Energy demand and the ability to meet it using efficient means are driving much of the innovation in the energy sector. One strategy to meet this demand is to develop energy storage and recovery devices. A device that has emerged recently that addresses the need for energy efficiency while also meeting power density requirements is the strain energy accumulator (SEA).

1.1. Pneumatic strain energy accumulator

The pneumatic form of the strain energy accumulator (pSEA) operates by capturing and storing the exhaust gas from one component until it is needed and used by another component at a later point in time. The pSEA functions by expanding a rubber bladder at a constant pressure inside a rigid shroud, storing energy in the form of both strain and pressure energy, and then contracts at a lower constant pressure returning the energy to the system to be used for a secondary task. Such a device would be useful in any industrial setting where the costly production of compressed air could be augmented by reusing pressurised exhaust air from one process to run other processes.

According to a 2012 Oak Ridge National Labs (ORNL) study, 70% of U.S. manufacturing facilities use a compressed air system and, on average, one-tenth of the energy used at those facilities goes towards powering industrial air compressors. Given that the fluid power industry averages only 22% efficiency (Love *et al.* 2012), and that the pneumatic sector is even less efficient (averaging just 15% efficiency), the need to develop efficient devices for compressed air energy storage and recovery is apparent.

One such application using the pSEA is the Ankle Foot Orthosis (AFO) stroke rehabilitation device (Boes *et al.* 2013). The AFO uses a rotary actuator powered by a compressed gas supply, carried by the patient, that helps raise and lower a patient's foot to improve muscle memory during rehabilitation. While changing multiple system parameters, efficiency increases ranging from 25 to 75% when using the pSEA on the AFO were reported. With no way to directly identify the efficiency increase due solely to the pSEA, a need to quantify system performance in terms of the SEA design parameters was identified. This need has motivated the current work to fully define and characterise an accumulator component efficiency model, and develop a lumped parameter state model to estimate system level efficiency improvements.

The ultimate goal for the current research is to accurately define efficiency increase limits that can be realised for various systems while using the pSEA. This paper demonstrates that the development of models for the pSEA has enabled the ability to provide estimates for efficiency limits at both the component and system level.

1.2. Pneumatic and strain energy literature survey

Initial investigation into the SEA by Pedchenko and Barth (2009) provided a proof of concept design of an energy dense SEA. In 2012, Tucker further investigated the energy density of the SEA device determining the forms of rubber that are ideal in terms of performance for use in the SEA due to their high energy density. In 2013, Boes *et al.* provided the first reported efficiency increases resulting from use of the pSEA. Equations to quantify these efficiencies are given in Cummins *et al.* 2015, offering the ability to characterise efficiency and how it relates to the unique material properties of rubber.

Prior to understanding the pSEA and how its performance benefits from the properties of rubber, a basic understanding of these properties is required. In his book Rubber Technology, John Dick (2009) provides a thorough overview of these properties including elasticity, tensile stress–strain behaviour and fatigue resistance, hysteresis, etc., which are the underlying operating principals of the pSEA. The Mullins effect is well documented in Mullins' original work from 1948 to explain how the strain of a rubber is dependent on previous loading, which is important for strain energy considerations. An often cited work by Cadwell *et al.* (1940) provides a comprehensive review of various parameters and their effect on the fatigue life of rubber showing how changing any one loading parameter can greatly affect the fatigue life of rubber. Current fatigue testing standards for rubber are given by ASTM 2011 and, specific to the SEA, understanding and characterising the ballooning behaviour of rubber tubing is presented in detail in Gent 1978 and 2005, corresponding to the behaviour observed in the ballooning process of the SEA. To obtain quantitative insights, standard uncertainty analysis such as that given in Haldar and Mahadevan (2000) can be used.

Harris *et al.* (2012) completed an efficiency optimisation study using current technologies and identified future needs of the pneumatic industry. Within the study, energy storage was specifically identified as an area for improvement. Additionally, future directions that were identified included the development of integrated performance metrics focused on model-based optimisation techniques tailored to specific applications. The three primary goals of the current research are to: (a) develop a generally applicable model-based component efficiency estimation as an integrated performance metric to the system efficiency, (b) experimentally measure the key

performance parameters of the pSEA including component efficiency, and expansion and contraction pressures for the specific system of interest, and (c) perform uncertainty analysis of the component performance parameters to make uncertainty propagation an integral part of system efficiency measurements.

2. Accumulator component efficiency model

The elastic bladder within the pSEA expands as incoming gas performs work and contracts when the gas is released, performing work on the gas. Compared to a fixed volume accumulator in which the accumulator's structure neither expands nor contracts and therefore can do no work on a gas, the total energy within the pSEA is stored in two different forms: the strain energy of the bladder and the pneumatic energy of the gas.

$$E_{\text{Tot}} = E_{\text{strain}} + E_{\text{pneumatic}} \quad (1)$$

The total strain energy absorbed while charging the accumulator is simply the work done by the gas as it expands into the accumulator:

$$E_{\text{strain}} = \int_{V_0}^{V_{\text{full}}} PdV \quad (2)$$

Above, V_0 and V_{full} represent the accumulator's initial and full volumes, respectively. The strain energy released during the accumulator's discharge is similar to the above integral with different limits of integration. Regarding the pneumatic potential energy of the gas within the accumulator, the following assumptions were made: (1) heat transfer conditions are assumed isothermal as the accumulator is filled and exhausted; (2) kinetic and potential energy (gravity) effects associated with the gas are negligible compared to other effects; and (3) the gas is assumed to be air and behaves as an ideal gas.

Once the accumulator is full, the mass of the air within the accumulator is fixed and, given the assumptions listed above, the pneumatic energy of the air can be determined by theoretically examining the air's potential to do work. Using the ideal gas law, for a fixed mass of air within the accumulator at a fixed temperature at any pressure and volume (including the maximum pressure, P_{max} , and full volume, V_{full} , of the fully charged accumulator, or the minimum pressure, P_{atm} , and final expanded volume, V_{final} , once the air has been exhausted from the accumulator), the following relation holds:

$$PV = P_{\text{max}} V_{\text{full}} = P_{\text{atm}} V_{\text{final}} = nRT = \text{Constant}$$

The work done by the air in the accumulator if it were to theoretically expand isothermally to a final volume (V_{final}) at a final pressure (atmospheric pressure, P_{atm}) is:

$$E_{\text{pneumatic}} = W = \int_{V_{\text{full}}}^{V_{\text{final}}} PdV$$

This expression can be rearranged with the ideal gas law:

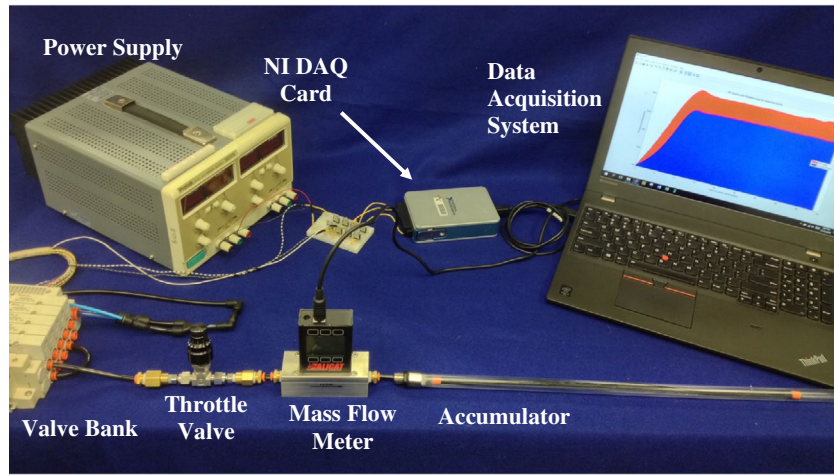


Figure 1. Component efficiency testing experimental test set-up.

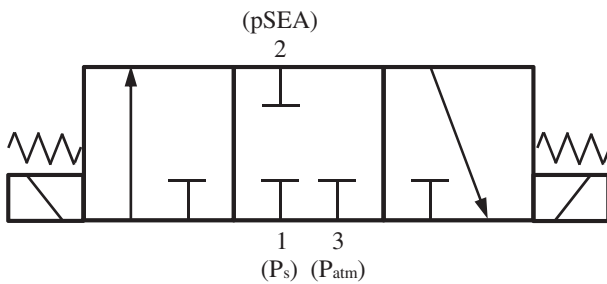


Figure 2. Schematic for automated valve for fill (left), hold (centre), and exhaust (right) positions.

$$\begin{aligned} E_{\text{pneumatic}} &= \int_{V_{\text{full}}}^{V_{\text{final}}} P dV = P_{\text{max}} V_{\text{full}} \int_{V_{\text{full}}}^{V_{\text{final}}} \frac{1}{V} dV \\ &= P_{\text{max}} V_{\text{full}} \ln \left(\frac{V_{\text{final}}}{V_{\text{full}}} \right) \end{aligned}$$

Using the ideal gas law, the ratio of final to full volume is equal to the ratio of the maximum pressure, experienced at the full volume of the accumulator, to atmospheric pressure. Therefore,

$$E_{\text{pneumatic}} = P_{\text{max}} V_{\text{full}} \ln \left(\frac{P_{\text{max}}}{P_{\text{atm}}} \right) \quad (3)$$

Thus, the total energy stored within the pSEA once it is fully expanded is:

$$E_{\text{Tot}} = \int_{V_0}^{V_{\text{full}}} P dV + P_{\text{max}} V_{\text{full}} \ln \left(\frac{P_{\text{max}}}{P_{\text{atm}}} \right) \quad (4)$$

The total energy stored by and extracted from the pSEA can be determined by evaluating the total energy function in Equation 2 at the respective limits of integration for the accumulator's fill and exhaust phases. A ratio of the energy output by the accumulator to the energy input into the accumulator yields the efficiency of the component, η_{acc} :

$$\eta_{\text{acc}} = \frac{- \int_{V_{\text{full}}}^{V_0} P dV + P_{\text{max}} V_{\text{full}} \ln \left(\frac{P_{\text{max}}}{P_{\text{atm}}} \right)}{\int_{V_0}^{V_{\text{full}}} P dV + P_{\text{max}} V_{\text{full}} \ln \left(\frac{P_{\text{max}}}{P_{\text{atm}}} \right)} \quad (5)$$

With the model-based analytical pSEA component efficiency estimate defined, experiments can be conducted to determine the pSEA component efficiency.

3. Efficiency experiments

Having developed the analytical equation necessary to determine the efficiency of the pSEA component, the necessary pressures and volumes, including the expansion and contraction pressures, can be experimentally measured and determined. The following describes the SEA's experimental set-up and demonstrates representative samples of the data acquired during the experiments.

3.1. Experimental set-up

The experimental set-up (Figure 1) consisted of a single pSEA, Alicat *M*-series Mass Flow Meter, throttle valve, Festo 5-way valve bank, supply pressure regulating valve (not pictured), electrical power supply and National Instruments (NI) data acquisition (DAQ) system. The pSEA tested in each series of tests consisted of an 18"-long, black, latex rubber tube (1/4" outer diameter, 1/8" inner diameter) encased by a 36"-long, transparent, polycarbonate shroud (5/8" outer diameter, 1/2" inner diameter).

Shop supply air (670 kPa) passed through the regulating valve where it was regulated down to approximately 360 kPa (denoted as P_s), which was subsequently connected to the supply port for the valve bank (port 1 in Figure 2). The upstream side of the mass flow meter was connected indirectly to port 2 on the opposite side of the bank. Between the mass flow meter and port 2 was the throttle valve. The throttle valve was placed in

line to keep the flow rate data to within the mass flow meter's operation limits. The valve bank was modified to create a 3-way valve that could be used to control the air flow into and out of the accumulator (Figure 2). All pressures are reported in absolute pressures.

In the hold phase (Figure 2, centre) all ports remained closed. During the fill phase (Figure 2, left), compressed air from supply flowed into the pSEA when port 1 diverted to port 2. Upon exhausting (Figure 2, right), air flowed from the pSEA out to atmosphere when port 2 diverted to port 3. Throughout the cycle, the mass flow meter was connected to the accumulator allowing the mass flow rate of the air flowing into and out of the accumulator to be measured. The mass flow meter also recorded pressure and temperature data simultaneously, and all sets of data were sent via a serial-to-USB cable to the laptop computer. The valve bank positioning was controlled by a 24 V electrical power supply controlled by a NI output DAQ card connected to the laptop computer.

One full cycle of the accumulator took 5 s and consisted of a primary hold stage (1.4 s), a fill stage (0.6 s), an intermediary hold stage (2 s), and finally, an exhaust stage (1 s). A LabVIEW interface was used to send and receive output and input signals from the DAQ card and mass flow meter, respectively, and control the test parameters. The mass-flow meter's sample rate was approximately 30 samples per second. To encourage uniform expansion during the fill stage, the rubber was pre-strained before testing by confining flow to its base portion until the base ballooned out. This pre-straining caused the material around the base to expand more easily relative to the rest of the rubber, so future ballooning would begin with the base and expand axially when the device was filled. The inner surface of the accumulator's shroud was also lubricated with medical-grade, water-soluble lubricant to further encourages the elastomer to expand and contract easily. Each accumulator test run consisted of 125 cycles, including a 25-cycle warmup period to minimise the Mullins effect followed by 100 cycles during which data were collected for analysis. A recovery period of 15 min was observed between each test.

3.2. Experimental data collection

Pressure, mass flow and temperature readings were acquired from the mass flow meter. The resulting time histories for three cycles for pressure, temperature and mass flow are shown in Figures 3–5, respectively.

Figure 3 exhibits behaviour similar to the results obtained in previous works (Gent 2005 and Pedchenko and Barth, 2009). Initially, a pressure spike is seen as the accumulator is made taut followed by a slight increase in pressure as the accumulator begins to balloon out. After ballooning initiates, the accumulator experiences a relatively constant expansion pressure. During the intermediate hold phase, a slight decrease in pressure over

time indicates a very minor, low-flow leak in the system. The pressure drops as the accumulator exhausts before experiencing a relatively constant contraction pressure and returning to atmospheric pressure.

Temperature fluctuated negligibly during a single cycle and for the eight tests considered, the greatest difference between the maximum and minimum recorded temperatures over a single cycle was only 0.11 °C, which confirms our assumption that the accumulator fills and exhausts under isothermal conditions. For the eight tests in aggregate, the difference between the overall minimum and overall maximum recorded temperatures was 1.3 °C.

Figure 5 shows the mass flow rate as a function of time where the positive spikes correspond to the fill stages and the negative spikes correspond to the exhaust stages. When the fill stage starts, the mass flow experiences a sharp rate increase as the bubble forms, demonstrates transient variation around a fill flow rate, and returns to zero once the accumulator is filled and the directional valve is closed. A small, negative mass flow is measured during the intermediate hold stage, further confirming the existence of a minor leak in the system. Behaviour similar to the fill phase is observed during exhaust phase of the pSEA, except having a negative mass flow rate with little transient variation.

Volume as a function of time is derived using the ideal gas law after the mass flow rate is integrated with respect to time. Integrating the mass flow data using the trapezoidal method of integration results in drift in the data due to aggregated uncertainty errors inherent in the mass flow meter's normal operation. Practically speaking, at a cycle's boundaries, the total integrated mass does not return to zero once the accumulator has filled and exhausted (Figure 6), which runs contrary to assumed conservation of mass. With the challenges associated with accurately measuring mass flow rate particularly in transient, dynamic and low flow conditions known (de Giorgi *et al.* 2008 and Igarashi *et al.* 2007) and given specified uncertainty within the mass flow meter's readings as published by the manufacturer, our presupposition that all mass entering the accumulator would also leave the accumulator is quantifiably justified since a final mass of zero falls within the range of possible values for the accumulator's total mass at the end of each cycle when aggregate uncertainty is also computed (Figure 6). Consequently, the integrated mass data were adjusted according to the following conditions: (1) each cycle's total mass should begin and end at zero; (2) later data points exhibit a greater range of uncertainty than earlier ones (due to aggregated error), thus later points could be displaced more from their original readings than earlier ones; and (3) the overall shape of the data may be scaled but should be maintained. The mass data were adjusted according to these parameters. A sample adjusted cycle's mass data are presented in Figure 7.

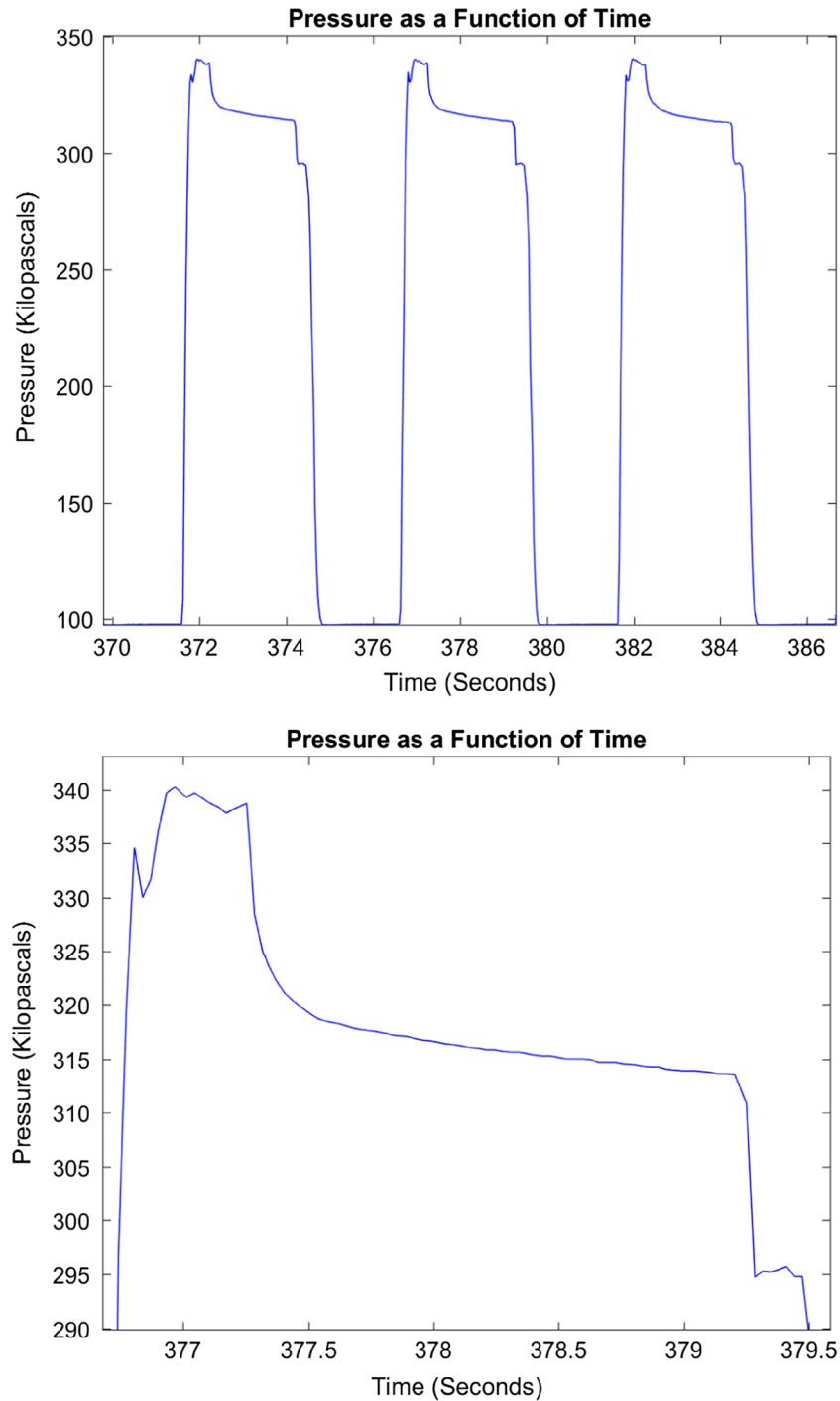


Figure 3. Pressure vs. time from three experimental cycles (above) and one cycle (below).

The integrated mass data were augmented with an estimate of the initial mass of air present in the accumulator prior to operation and after applying the ideal gas law using measured pressure and temperature data for every instance of time, volume data for the accumulator was derived (Figure 8).

By combining pressure and volume data at each instant in time, pressure–volume curves for each cycle were generated. Data within a cycle were divided into fill and exhaust phases with respect to the cycle's maximum and minimum volumes: data produced as the system moved from a minimum volume to a maximum volume

was designated as the fill phase (red), while data produced as the system moved from a maximum volume to a minimum volume was designated as the exhaust phase (blue). Sample pressure–volume curves for the beginning (cycle 1), middle (cycle 50), and end (cycle 100) cycles from a 100-cycle test are shown in Figure 9.

The accumulator's energy storage capacity benefits from the hyperelastic behaviour of rubber. As the rubber is stretched it softens and is able to stretch further during subsequent cycles under the same input conditions. As the rubber stretches to greater volumetric displacements, the accumulator is able to store greater amounts of strain

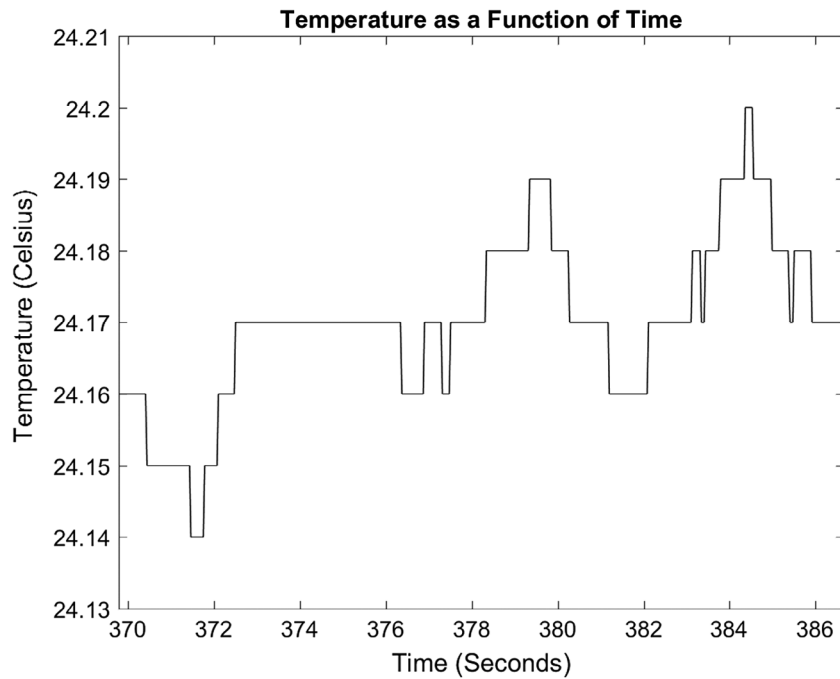


Figure 4. Temperature vs. time from three experimental cycles.

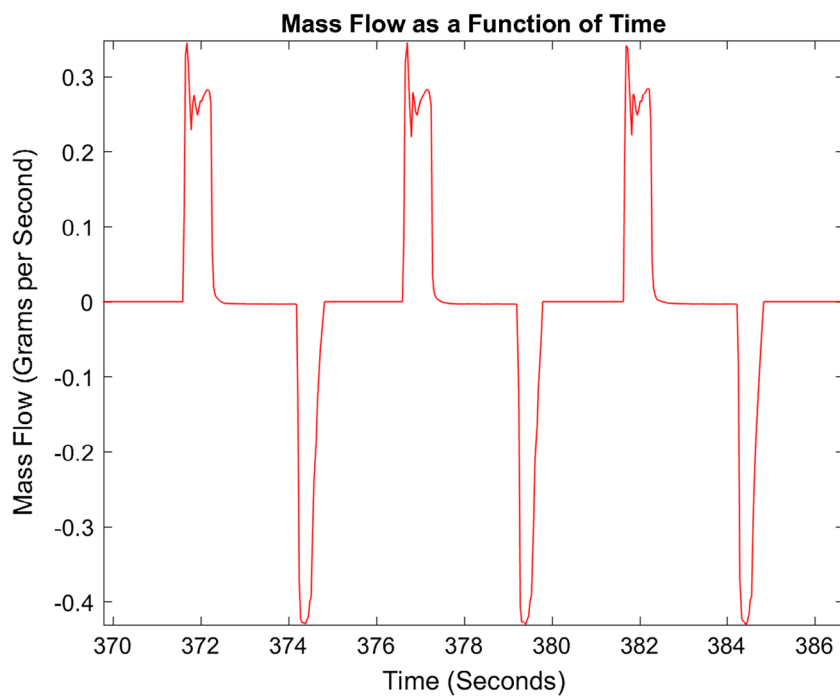


Figure 5. Mass flow vs. time from three experimental cycles.

energy as more area under the PV curve is encompassed (Eqn. 4). Finally, assuming no change in maximum pressure, a greater full volume, V_{full} , of the accumulator would result in greater pneumatic energy stored in the accumulator (Equation 3). From these observations we can see that the accumulator can store more energy during later cycles than during earlier ones over the course of a single test.

It should be noted that though the accumulator stretched to greater volumes over the course of a test, it

was never allowed to fill the entire volume of the outer rigid shroud. Doing so would result in a late-cycle pressure spike as mass continued to enter the system while the accumulator was completely filled. There is evidence that this scenario produces greater efficiency and allows more energy to be stored in the accumulator, however, the trade-off is potential premature device failure, a result that was experienced during testing at excess pressures and indicates the importance of properly designing the accumulator to the desired engineering application.

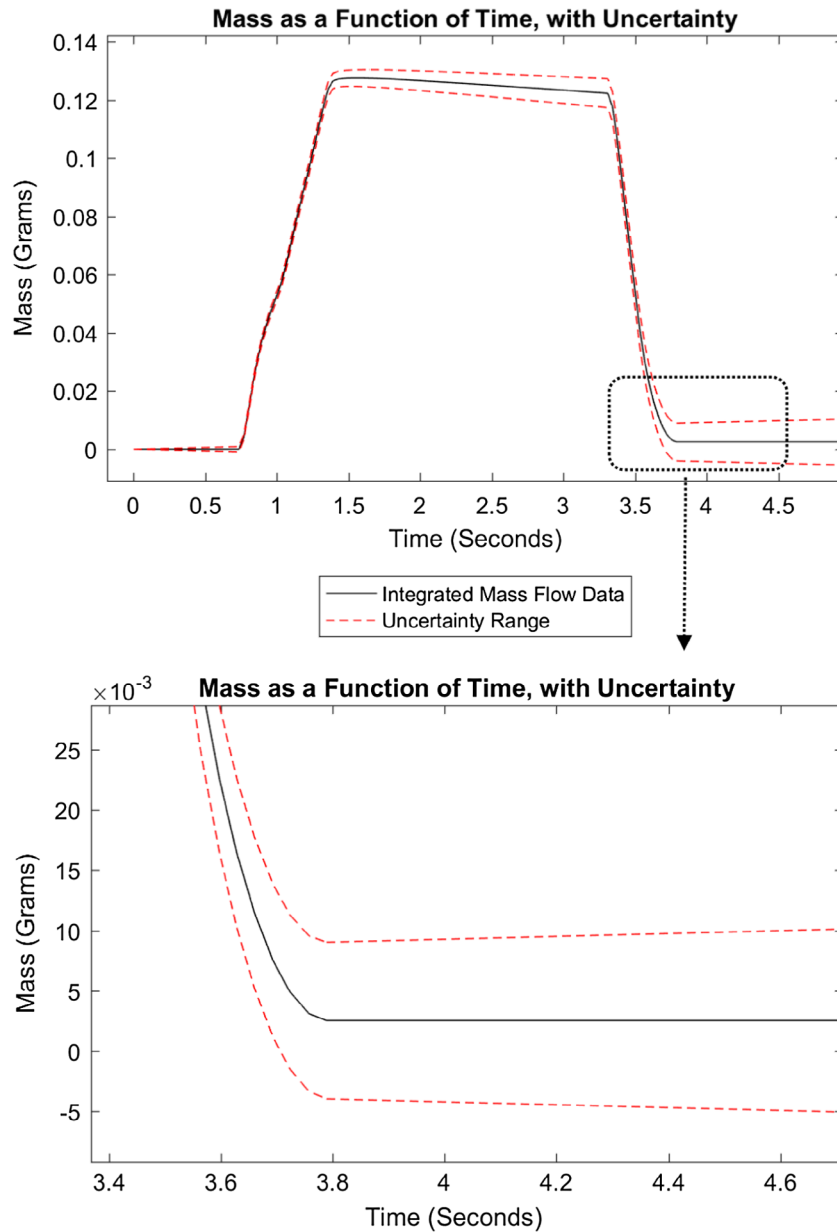


Figure 6. Mass vs. time from one experimental cycle with computed uncertainty range shown.

4. Results and discussion

4.1. Component efficiency

A cycle's efficiency is defined as the ratio between the total energy output by the pSEA to the total energy input to the pSEA as given in Equation 5. The total energy is determined in part by calculating the area under the pressure–volume curve, or the strain energy, for both the fill and exhaust phases. This area was determined by integrating pressure with respect to volume using the trapezoidal method and is shown in Figure 10.

The remainder of the total energy comes from the maximum potential of the pressurised air and is determined by measuring the cycle's maximum volume and corresponding maximum pressure at that volume. By combining the maximum potential energy of the pressurised air with the strain energy, for both fill and exhaust phases, the total input and output energy are determined

and by dividing the former from the latter, the efficiency of the cycle is obtained. Calculated efficiency values for 8, 100-cycle tests are depicted in Figure 11.

4.2. Component efficiency uncertainty analysis

The mean value for each of the 100-cycle tests, μ , along with the standard deviation, σ , and standard deviation of the mean, SD_{μ} , were calculated as follows:

$$\mu = \frac{1}{n} \sum_{i=1}^n x_i \quad (6)$$

$$\sigma = \left[\frac{1}{n-1} \sum_{i=1}^n (x_i - \mu_x)^2 \right]^{1/2} \quad (7)$$

$$SD_{\mu} = \sigma / \sqrt{n} \quad (8)$$

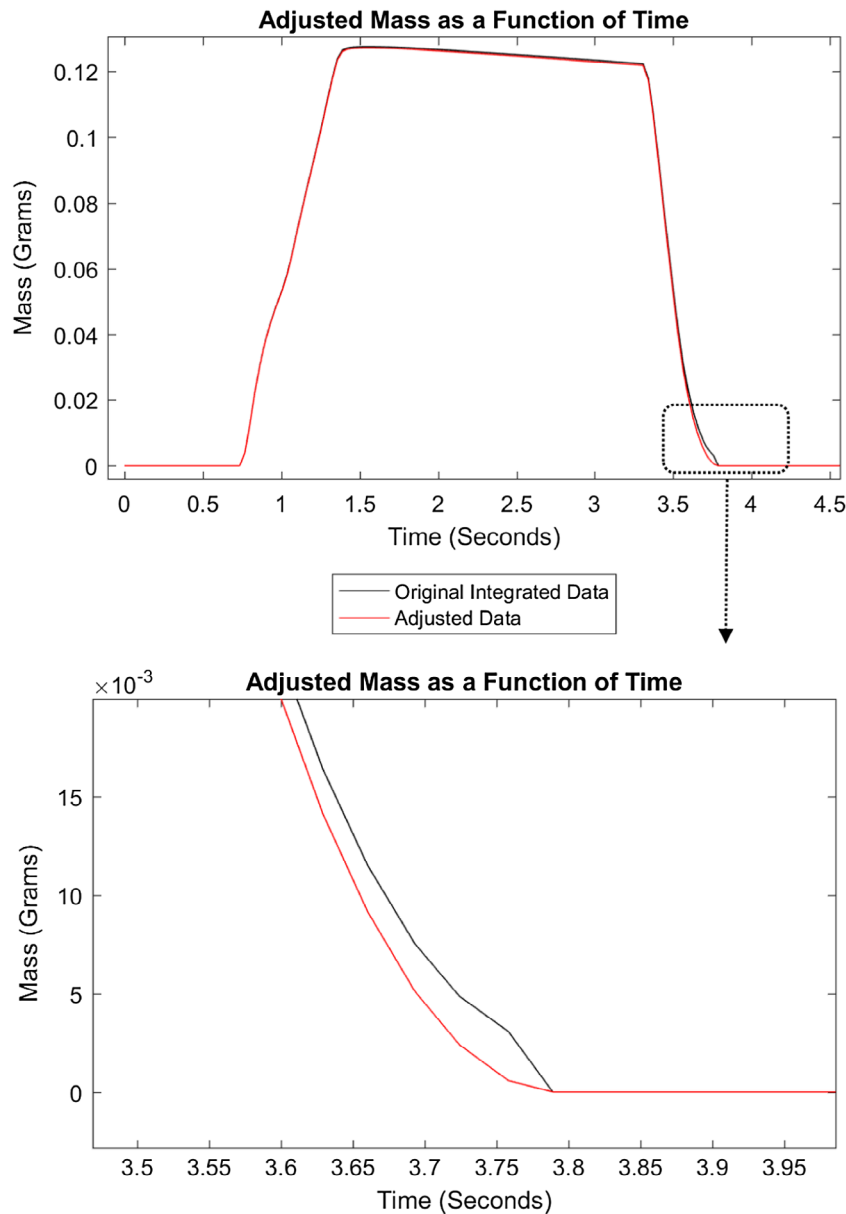


Figure 7. Corrected mass vs. time from one experimental cycle.

where n is the total number of data points and x_i is value of the i th data point. The experimentally determined efficiency values for the pSEA component from Figure 11 exhibit little to no trend over time, and thus a basic mean and standard deviation evaluation are sufficient for analysis. The results are given in Table 1.

In Table 1, the 8 Cycle Average refers to taking all 8, 100-cycle tests and treating them as a single data-set. The resulting values correspond to a composite value for the pSEA component across tests. Uncertainty analysis indicates that across all tests the pSEA as a component has an average efficiency around 93.6%, with a standard deviation of 0.4%. Even when the warmup cycles are taken into consideration (observed but not shown for conciseness) average efficiency is still above 93%, and in both cases the standard deviation is around 4 tenths of a per cent. This indicates that in spite of hysteresis and the Mullins effect, which often times negatively affect elastomer performance, the pSEA is still an energy efficient device.

4.3. Mullins effect and energy storage capacity

The Mullins effect's impact on the accumulator's performance is most clearly seen in Figure 12 which shows a distinct change in the accumulator's performance over time. Two trends are apparent: first, during the first and second tests, the accumulator was able to reach a higher maximum volume for each cycle than in any later test, in accordance with the Mullins effect. Subsequent cycles required more energy to stretch the elastomer and accordingly, we believe tests 3–8 characterise the accumulator's steady-state performance more faithfully. During steady-state performance we see a second trend in the data: the elastomer tended to reach higher volumes over the course of a test and higher still in subsequent tests, which can be attributed to the decrease in hysteresis over time as is established and discussed in the literature. Such volumetric gains appear to be limited and future tests would probably not

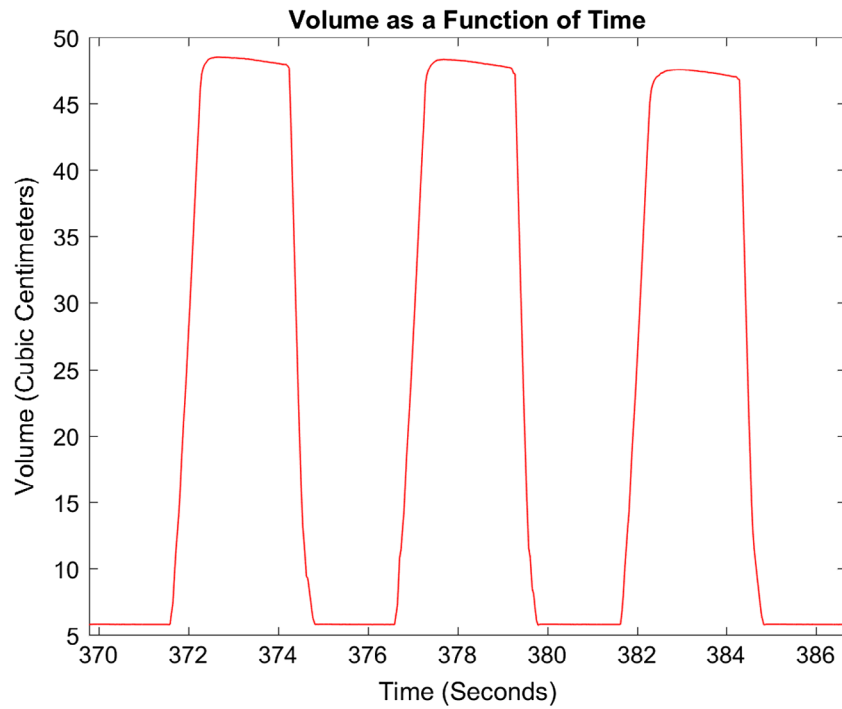


Figure 8. Volume vs. time data for three experimental cycles.

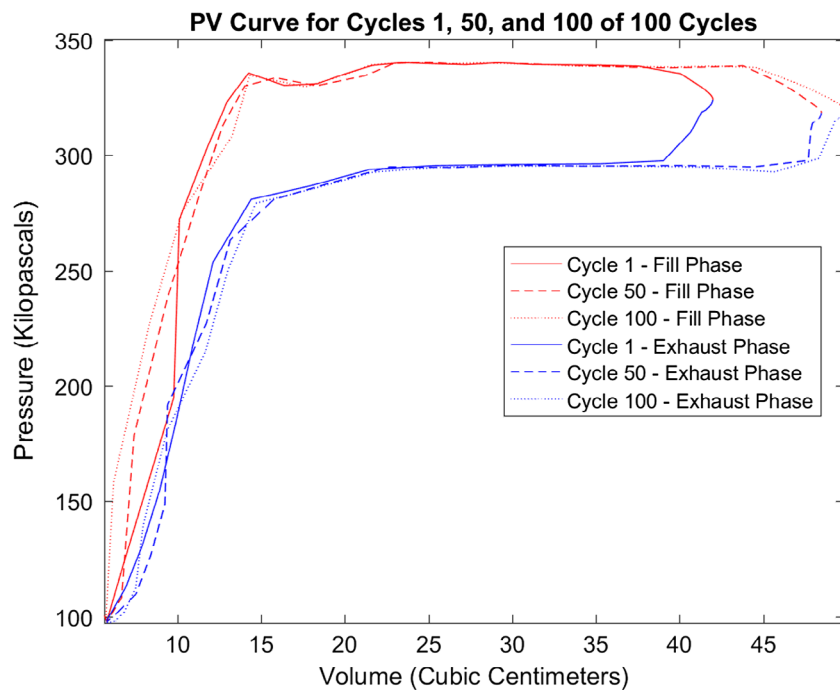


Figure 9. Pressure vs. volume for cycles at the beginning, middle and end of a 100-cycle test.

yield the same maximum volumes such as in the first two tests. Incidentally, though the accumulator doesn't fill to the same maximum volume during tests 3–8 and, therefore, does not store as much energy as in earlier tests, it doesn't experience any drop in efficiency. In fact, efficiency actually increases slightly as the accumulator approaches steady-state performance (Table 1).

Figure 13 demonstrates how the Mullins effect influences the total energy the accumulator is able to store

and release over time. As discussed in Section 3.2, since the accumulator's energy storage capacity results from changes in the accumulator's maximum volume, it's unsurprising that trends in the energy data should closely follow trends in the maximum volume data. The energy input and output of each cycle appeared to have hit a limit by the last three tests and by averaging the data in those tests, we determined that an accumulator of this size operating under our pre-defined conditions (source

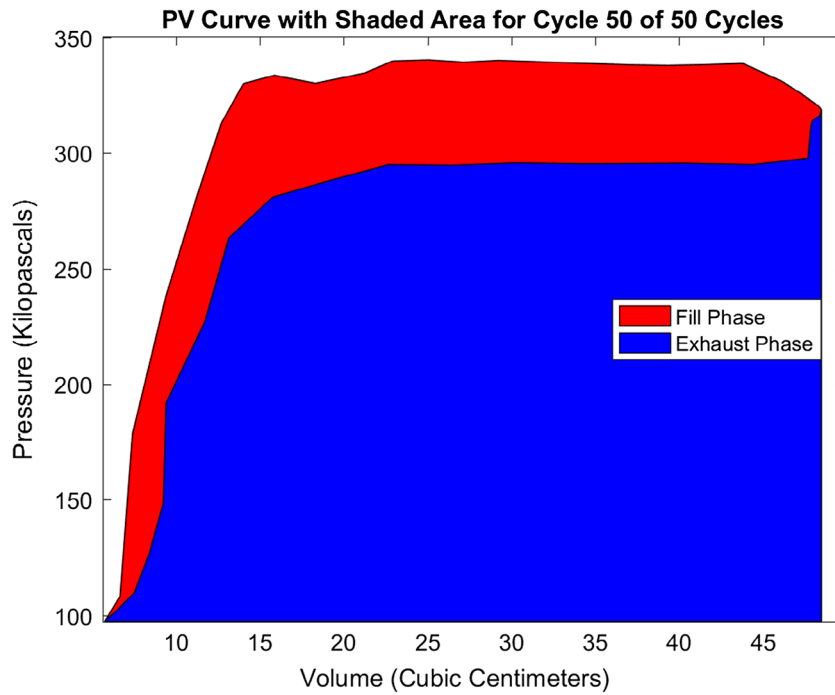


Figure 10. Pressure volume plot showing strain energy in (red + blue) and out (blue) of pSEA.

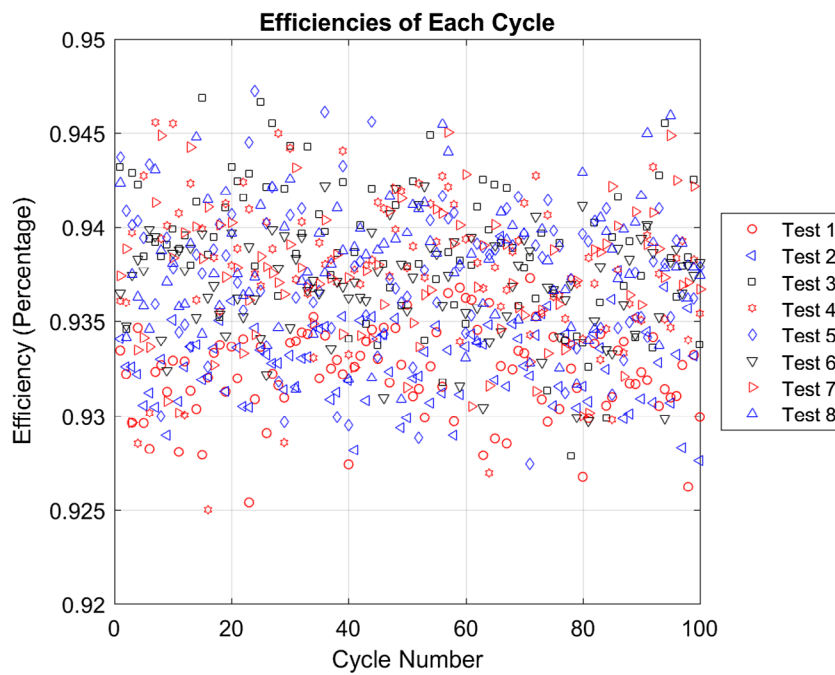


Figure 11. Energy efficiency of pSEA component for 8, 100 cycle tests.

Table 1. Component experimental efficiency of pSEA.

Strain energy accumulator component efficiency		
Trial	Mean (%)	Standard deviation (%)
1	93.22	0.237
2	93.28	0.214
3	93.87	0.361
4	93.77	0.386
5	93.75	0.380
6	93.69	0.274
7	93.72	0.360
8	93.80	0.324
8 cycle average	93.64	0.396

pressure of approximately 3.6 bar, fill time of 0.6 s) could store approximately 37.61 ± 0.07 joules of energy and release approximately 35.26 ± 0.07 joules of energy.

4.4. Component key performance parameters

In order to study the accumulator’s impact on system efficiency, it is first necessary to determine the pSEA’s key performance parameters: the expansion and contraction pressures. These pressure values will serve as input parameters to the system efficiency model. The

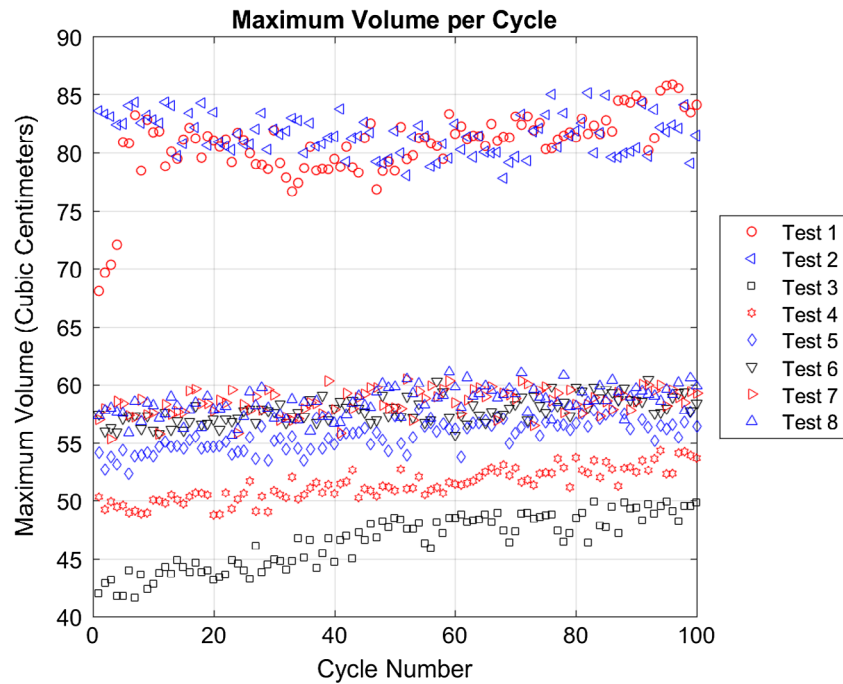


Figure 12. Maximum volume per cycle over eight tests.

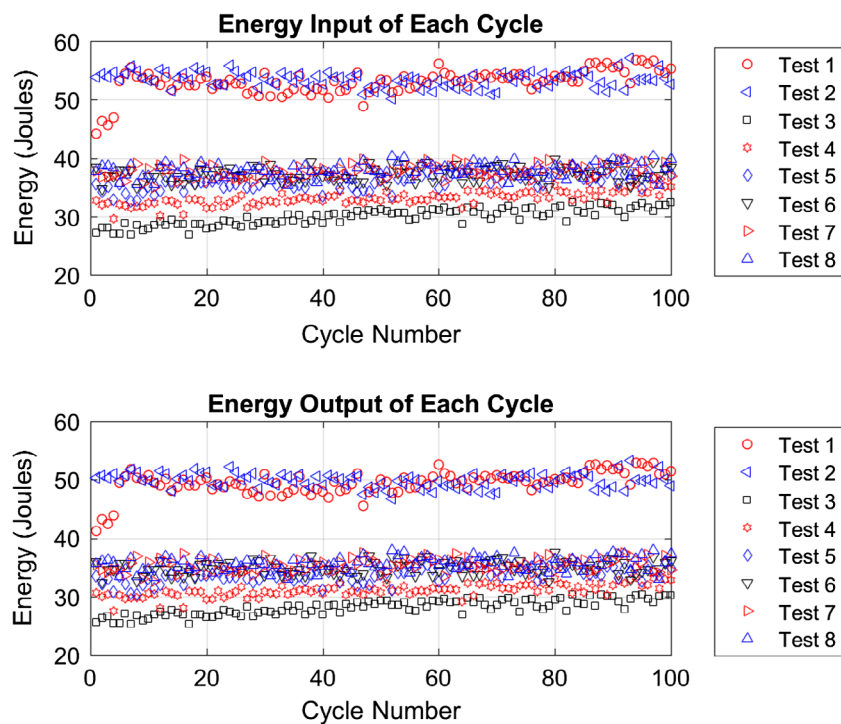


Figure 13. Energy into pSEA (top) and energy out of pSEA (bottom).

expansion pressure of the pSEA is characterised by a rapid increase in volume while the pressure remains relatively constant. Likewise, the contraction pressure corresponds to a rapid decrease in volume at a relatively constant pressure. Both of those pressures can be clearly seen on a pressure–volume diagram in Figure 9 as the regions where the curve is nearly linear with very little slope. In the constant pressure region, minimum and maximum volumes were set as end points for determining the expansion and contraction pressures. The pressure data between those points were averaged during

each of the fill and exhaust phases. A sample determination is given in Figure 14. The experimentally determined expansion and contraction pressures for the 8, 100-cycle tests are shown in Figure 15.

Like the energy in/out data, the expansion and contraction pressures change over time with clear differences between values obtained during the first two tests and later tests, as expected due to the Mullins effect. One difference between Figures 15 and 13 is that during the last six tests (indicative of the accumulator's steady-state performance) the energy in/out appears to be increasing

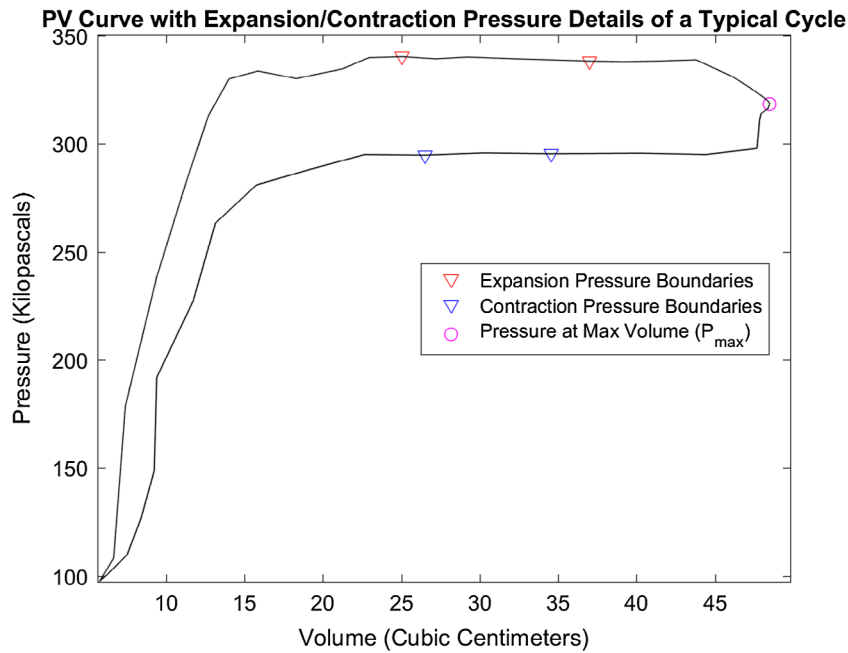


Figure 14. Points on P-V curve used to determine expansion, contraction, and maximum pressures.

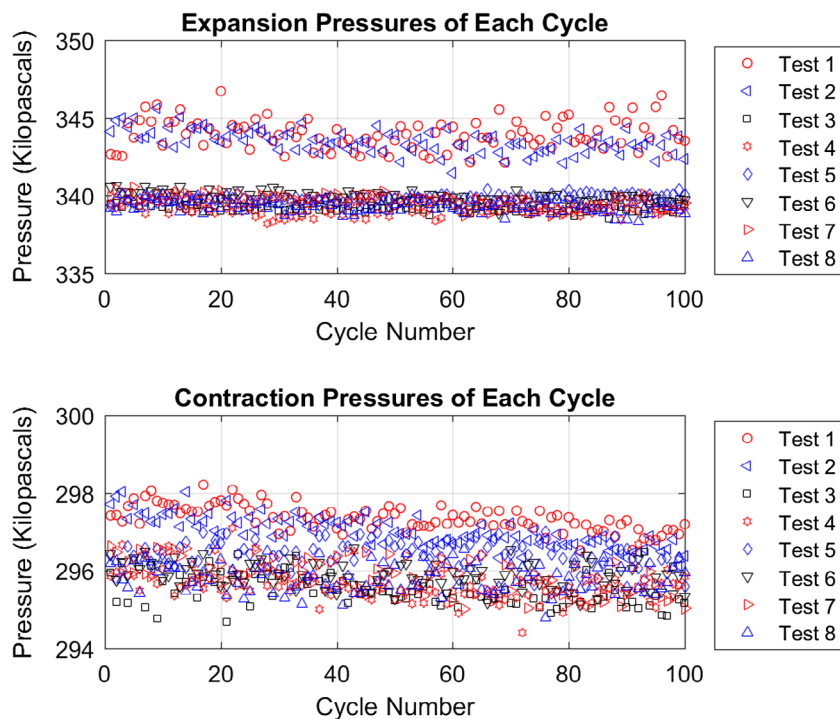


Figure 15. Expansion (top) and contraction (bottom) pressures for 8, 100-cycle tests.

with each cycle and with each successive test until it approaches a limit, whereas the expansion and contraction pressures appear to have already reached a limit and only slightly decrease over the course of a test. This indicates that while the accumulator expands to greater volumes during steady-state operation, thus storing more energy, its expansion and contraction pressures remain relatively fixed. The steady-state expansion and contraction pressures, determined from the mean and standard deviation of the mean of the final three tests, were

determined to be 339.61 ± 0.03 and 295.85 ± 0.02 kPa, respectively.

5. Conclusions and future work

At the commencement of the study, three primary objectives were identified. The first was to develop a generally applicable model-based efficiency estimate as an integrated performance metric to the system efficiency. Starting with a simple energy balance, a model-based

equation for the efficiency of the pSEA component was developed and is given in Equation 5. This general model-based methodology enables individual component efficiency to be an integrated performance metric to system efficiency for both pneumatic and strain energy systems.

The next objective was to experimentally measure the key performance parameters of the pSEA including component efficiency and expansion and contraction pressures. The pSEA steady state component efficiency was experimentally determined to be consistently over 93% and the expansion and contraction pressures were also found to asymptotically approach steady state values of 339.6 and 295.9 kPa, respectively.

The final objective was to perform uncertainty analysis of the component performance parameters to identify sources of uncertainty and make uncertainty propagation an integral part of system efficiency measurements. Mean value of the component steady-state efficiency was found to have a maximum standard deviation of less than 0.4%, and the calculated steady-state expansion and contraction pressures demonstrated negligible error from their mean values. Having obtained all three objectives, the component model, performance metrics and uncertainty analysis, enables development and testing of a system model with corresponding performance metrics using an integrated approach. With the pneumatic sector of the fluid power industry averaging only 15% efficiency, introducing the pSEA having 93% efficiency into existing fluid power systems has the potential to substantially impact pneumatic systems efficiency.

Acknowledgements

The authors would like to thank SMC Corporation for their donation of equipment to improve the experimental test set-up, shown in the experimental set-up section, for the system efficiency testing currently underway and discussed in the future work section. Finally, the authors would like to thank Dr. Janette Meyer for her review of the manuscript in preparation for submission to the journal.

Disclosure statement

No potential conflict of interest was reported by the authors.

Funding

This work was supported by the Center for Compact and Efficient Fluid Power, an NSF Engineering Research Center [grant number EEC-0540834].

Notes on contributors



Joshua J. Cummins received his BSME and MSME from Purdue University in 2007 and 2010, respectively. Cummins worked as a Rotary Wing Structures Engineer in the Airframe Technology branch of the Naval Air Systems Command from 2010 to 2013. Cummins resumed graduate studies in Fall 2013 at Vanderbilt University as a graduate

research assistant at the Laboratory for Systems Integrity and Reliability (LASIR) where he expects to complete his PhD in Mechanical Engineering in May 2016.



Seth Thomas received his BA in International Studies and Writing from the University of Central Arkansas in 2008. After serving in the Peace Corps from 2011 to 2013 and motivated by his experiences during his time there, Seth made a career change and returned to the University of Central Arkansas to pursue a BS in Applied Physics where he expects to graduate in May 2016. Seth plans to start graduate studies in Engineering in Fall 2016.



Christopher J. Nash expects to receive his BS in Mechanical Engineering, with a minor in Materials Science Engineering, in May 2016 from Vanderbilt University. Chris is currently an undergraduate research assistant in the Laboratory for the Design and Control of Energetic Systems (DCES) and the Laboratory for Systems Integrity and Reliability (LASIR) at Vanderbilt University. Chris plans to start graduate studies in Fall 2016.



Sankaran Mahadevan received his BS from the Indian Institute of Technology, his MS from Rensselaer Polytechnic Institute and Ph.D. from Georgia Institute of Technology all in the area of Civil and Environmental Engineering. Mahadevan is currently the John R Murray Sr. Professor of Civil and Environmental Engineering at Vanderbilt University. Mahadevan's research interests include reliability and uncertainty analysis methods, material degradation, structural health monitoring, design optimisation, and model uncertainty for civil, mechanical and aerospace systems.



Douglas E. Adams received his BSME from the University of Cincinnati, MSME from the Massachusetts Institute of Technology and PhD from the University of Cincinnati. Adams is currently the Daniel E. Flowers Distinguished Professor and Chair of the Civil and Environmental Engineering Department. Adams research interests include nonlinear structural dynamics and vibrations, structural health monitoring/diagnostics and damage prognosis, and noise and vibration control in the areas of aerospace, automotive, energy, and defence systems.



Eric J. Barth received his BS degree in engineering physics from the University of California at Berkeley, and his MS and PhD degrees from the Georgia Institute of Technology in Mechanical Engineering. Barth is currently an Assistant Professor of Mechanical Engineering at Vanderbilt University. Barth's research interests include design, modelling and control of fluid power systems, and actuator development for autonomous robots.

ORCID

Seth Thomas  <http://orcid.org/0000-0003-1006-1731>

Christopher J. Nash  <http://orcid.org/0000-0002-1504-8563>
 Sankaran Mahadevan  <http://orcid.org/0000-0003-1969-2388>
 Eric J. Barth  <http://orcid.org/0000-0002-7462-3417>

References

- ASTM, 2011. *ASTM D4482-11, Test method for rubber property – extension cycling fatigue*. West Conshohocken, PA: ASTM International. doi:10.1520/D4482-11.
- Boes, M.K., et al., 2013. Fuel efficiency of a portable powered ankle-foot orthosis. In: *Proceedings of the IEEE 13th international conference on rehabilitation robotics (ICORR 2013)*, 24–26 June Seattle, WA, 1–6.
- Cadwell, S.M., et al., 1940. Dynamic fatigue life of rubber. *Industrial and engineering chemistry*, 12, 19–23.
- Cummins, J.J., Barth, E.J. and Adams, D.E., 2015. Modeling of a pneumatic strain energy accumulator for variable system configurations with quantified projections of energy efficiency increases. In: *Proceedings of the 2015 Bath/ASME symposium on fluid power and motion control*, 14 October Chicago, IL. New York, NY: American Society of Mechanical Engineers, V001T01A055–8.
- Dick, J.S., 2009. *Rubber technology compounding and testing for performance*. 2nd ed. Cincinnati, OH: Hanser Publications.
- Gent, A.N., 1978. Rubber elasticity: basic concepts and behavior. In: F.R. Eirich, ed. *Science and technology of rubber*. 3rd ed. New York, NY: Academic Press, 1–21.
- Gent, A.N., 2005. Elastic instabilities in rubber. *International journal of non-linear mechanics*, 40, 165–175.
- de Giorgi, R., et al., 2008. Thermal model of a tank for simulation and mass flow rate characterization purposes. In: *Proceedings of the 7th JFPS international symposium on fluid power*, 15–18 September Toyama, JA, 226–230.
- Haldar, A. and Mahadevan, S., 2000. *Probability, reliability and statistical methods in engineering design*. New York, NY: Wiley.
- Harris, P., O'Donnell, G.E. and Whelan, T., 2012. Energy efficiency in pneumatic production systems: state of the art and future directions. In: D. Dornfeld, and B. Linke, eds. *Proceedings of the 19th CIRP international conference on life cycle engineering*, 23–25 May Berkeley, CA: Springer Science & Business Media, Heidelberg, 363–368.
- Igarashi, K., Kawashima, K. and Kagawa, T., 2007. Development of simultaneous measurement system for instantaneous density, viscosity and flow rate of gases. *Sensors and actuators A*, 140, 1–7.
- Love, L.J., Lanke, E. and Alles, P., 2012. *Estimating the impact (energy, emissions and economics) of the U.S. fluid power industry*. Oak Ridge, TN: Oak Ridge National Laboratory.
- Mullins, L., 1948. Effect of stretching on the properties of rubber. *Rubber chemistry and technology*, 21, 281–300.
- Pedchenko, A. and Barth, E.J., 2009. Design and validation of a high energy density elastic accumulator using polyurethane. In: *Proceedings of the 2009 ASME dynamic systems and control conference*, 12–14 October 2009 Hollywood, CA, New York, NY: American Society of Mechanical Engineers, 283–290.
- Tucker, J., 2012. *Design and experimental evaluation of a high energy density elastomeric strain energy accumulator*. Thesis (MS). Vanderbilt University.